

## Nanoscale Pattern Formation in Non-Equilibrium Surface Chemical Reactions

Y. DE DECKER<sup>1</sup> and A. S. MIKHAILOV<sup>2</sup>

<sup>1</sup>*Center for Nonlinear Phenomena and Complex Systems, Université Libre de Bruxelles, Campus Plaine, C.P. 231, B-1050 Brussels, Belgium*

<sup>2</sup>*Abteilung Physikalische Chemie, Fritz-Haber-Institut der Max-Planck-Gesellschaft, Faradayweg 4-6, 14195 Berlin, Germany*

Using examples from surface science, we consider in this article problems of non-equilibrium pattern formation in reactive soft matter. An interplay of reaction, diffusion and energetic interactions between adatoms can produce a variety of non-equilibrium nanostructures, both stationary and traveling. These structures are similar to the patterns found in phase-separating binary mixtures under the influence of reactions. Because of their small sizes, such nanostructures are significantly affected by fluctuations. The derivation of mesoscopic stochastic equations for fluctuating concentrations, starting from the microscopic master equation of the lattice approximation, is discussed. Special attention is paid to surface chemical reactions involving a promoter species, where experimental observations are available.

### §1. Introduction

Catalytic surface reactions maintained far from equilibrium are well known to contain all the necessary ingredients in order to generate complex phenomena and dissipative structures. Experimentally, a rich variety of spatiotemporal patterns has been discovered<sup>1),2)</sup> (such as waves, spirals, turbulence, ...) for which the characteristic length scales lies in the range of tens of micrometers and that can therefore be considered as effectively macroscopic phenomena. The recent development of experimental tools providing a nearly atomic spatial resolution has however revealed that non-equilibrium structures can also appear at much shorter scales, ranging from a few micrometers down to the order of the nanometer.<sup>3)-5)</sup> The large-scale properties corresponding to such reactive systems, like the global reactivity or selectivity of the process, are in general expected to depend strongly on such a nanoscopic pattern formation. In this view, it appears that controlling the onset and the properties of self-organized nanostructures through an appropriate choice of macroscopic parameters can lead in general to a better engineering of surface reactions. It is necessary in order to achieve this goal to develop theoretical approaches allowing for the understanding of the essential underlying processes.

Recent theoretical developments have led to the idea that the combination of non-equilibrium chemical reactions and energetic interactions between the particles can give birth to structures whose characteristic size lies well beyond the diffusion length of the species involved.<sup>6)-9)</sup> This has been seen, for example, in simulations of phase-separating binary mixtures of reactants and in experiments involving polymer blends. In the specific case of surface chemical reactions, potential interactions are in general expected to be present, and often result from direct and indirect (substrate-

mediated) contributions. These interactions are usually strong and can extend from several Angströms to a few nanometers, providing thus cohesion between particles at short distances.<sup>10),11)</sup>

There exist several levels of description in order to describe the dynamical behaviors associated with such systems. Since surface chemical reactions involve the rearrangement of electrons between adsorbed atoms or molecules, a first-principle approach would be of course desirable, so that the global dynamics of these systems can be deduced directly from quantum mechanics. This is nothing but the ultimate goal of non-equilibrium statistical mechanics; despite recent impressive theoretical advances in this field and increasing available computer capability, this “state-of-the-art” approach cannot however be considered yet as a practical tool in the case of complex systems. Alternatively, one can consider a simplified microscopic picture of the reality in which the molecules are involved in elementary chemical events seen as are fluctuating, Markov processes.

In this view, the dynamics of surface reactions can be characterized by a Glauber-type master equation giving the time evolution for the probability to find the surface in a given configuration. The transition probabilities between surface states typically depend on the local configuration of adsorbates and on the details of energetic interactions between particles. Starting from this master equation, a coarse-graining of the surface can be introduced by dividing it into boxes, for which a *local and fluctuating* concentration can be defined [see Ref. 13)]. The spatiotemporal evolution of the surface concentrations obeys then a Langevin-like equation which forms the starting point of our description. This approach has been applied to numerous examples of surface reactions, revealing the spontaneous formation of nanostructures.<sup>13)–15),17),19)</sup> When the size of the sub-domains becomes significant, these stochastic equations take the form of mesoscopic reaction-diffusion equations for the coverages<sup>12),16),18)</sup> where the effects of energetic interactions are still present and directly deduced from the microscopic picture of the master equation.

To illustrate this we first present in §1 some simple examples of systems involving adsorbates with lateral interactions. For the case of a single species on a lattice,<sup>13)</sup> we discuss the derivation of the stochastic evolution equation from the knowledge of the microscopic details and the limits of validity for which we expect this approach to be correct. The deterministic limit of this equation corresponding to the mean field approximation is also obtained, in which the energetic interactions influence the rates of the elementary processes. A particular emphasis is placed on the unusual diffusion term emerging from this derivation and on the phase transition leading to the coexistence of a dense and a dilute phase. In a second example, an annihilation reaction involving two interacting reactants is considered.<sup>17)</sup> Interestingly, much more complex spatiotemporal phenomena are observed in this case, such as stationary and travelling nanostructures whose length scale can be analytically estimated.

In the second section, we consider the case of surface reactions in the presence of a co-adsorbed, non-reactive additional species.<sup>20),21)</sup> This situation is often met in real-world heterogeneous catalytic systems: promoters or poisons are co-adsorbed species that do not react directly but can locally enhance or decrease the reaction

rates and usually have strong lateral interactions with the other particles.<sup>22)</sup> This class of systems forms an important illustration of the combination of far from equilibrium reactions and energetic interactions and recent experimental results confirm the formation of structures of a few micrometers under reaction condition.<sup>21), 23)–25)</sup> To illustrate the origin of this phenomenon, we show, using a simple general model, that these kinds of systems can in general spontaneously organize themselves into such microstructures, resulting in a strong modification of the global activity of the surface reaction. In the third section, the effects associated with different mechanisms of diffusion are discussed and exemplified with the case of promoted surface reactions. We will finish by discussing how important it is in our view to control the formation of patterns at such a nanoscopic level in the case of surface processes and how mesoscopic approaches like the one we use can help in doing so.

## §2. Towards a mesoscopic description of surface processes

Before considering some examples of specific surface processes, we first focus on the generic properties of the microscopic lattice model forming the basis of the mesoscopic theory. In this approach the surface is seen as a lattice with a specific geometry, the nodes of which can be occupied by an adsorbed molecule. Multiple occupation of the sites is forbidden, so that the local occupation numbers  $n_\alpha(\mathbf{R})$  can only take the values 0 or 1. The dynamical evolution of this boolean variable is dictated by the occurrence of different possible events: adsorption, desorption, diffusion, reaction, etc. These processes are considered here as stochastic and Markovian, so that one expects the time evolution of the joint probability distribution  $P(\{n_\alpha(\mathbf{R})\}, t)$  for a microscopic configuration  $\{n_\alpha(\mathbf{R})\}$  to be given by a Glauber-type master equation of the form

$$\frac{d}{dt} P(\{n_\alpha(\mathbf{R})\}, t) = \sum_{\{n'_\alpha(\mathbf{R})\}} \sum_{\rho} [w_\rho(\{n'_\alpha(\mathbf{R})\} \rightarrow \{n_\alpha(\mathbf{R})\}) P(\{n'_\alpha(\mathbf{R})\}, t) - w_\rho(\{n_\alpha(\mathbf{R})\} \rightarrow \{n'_\alpha(\mathbf{R})\}) P(\{n_\alpha(\mathbf{R})\}, t)], \quad (2.1)$$

where the sums run, respectively, over configurations and events. The choice the transition probabilities  $w_\rho$  is of course not arbitrary: they must reflect what is known about the microscopic mechanism of the corresponding elementary event, take into account the presence of energetic interactions and must in addition respect detailed balance at equilibrium.

Generally speaking, an analytic resolution of such a master equation is only rarely feasible. Usually, it is possible to derive under certain approximations quantities such as the time evolution of the (spatially averaged) coverage or any probability to find on the lattice clusters of a given size. The approach used here is slightly different, as will be now exemplified on a first, simple example.

### 2.1. Phase separation for a single interacting adsorbate

We first analyze the case of a single gaseous species  $A$  capable of adsorbing, desorbing and diffusing on the nodes of a surface.<sup>13)</sup> As we mentioned before,

the rates of the different elementary processes must reflect the fact that any adsorbed particle  $A_{(\text{ads})}$  located at  $\mathbf{R}$  experiences a global interaction potential  $U(\mathbf{R}) = -\sum_{\mathbf{R}'} u(\mathbf{R}' - \mathbf{R}) n(\mathbf{R}')$  where  $u(\mathbf{R}' - \mathbf{R})$  is the binary interaction potential and  $n(\mathbf{R}')$  the local occupation by  $A_{(\text{ads})}$  at site  $\mathbf{R}'$ . The exact form of the pairwise interaction potentials in a given reactive system should be specific and determined by a corresponding microscopic analysis. For the sake of illustration, we will consider in this case and in the following examples Gaussian interactions of the form

$$u(\mathbf{R} - \mathbf{R}') = \frac{u_0}{(\pi r_0^2)^{d/2}} \exp\left(-\frac{|\mathbf{r} - \mathbf{r}'|^2}{r_0^2}\right). \quad (2.2)$$

In this equation,  $r_0$  is a characteristic interaction radius and the coefficient  $u_0$  specifies the interaction intensity. Note that positive values of  $u_0$  correspond to attraction and negative values to repulsion between the considered particles. The parameter  $d = 1, 2$  is the medium dimensionality (some of our numerical simulations shall be performed for a one-dimensional system).

On the basis of this model, one can construct the transition probabilities associated with the different elementary processes. For adsorption, we choose to adopt the simple Langmuir-type rate  $w_a(\mathbf{R}) = k_a p (1 - n(\mathbf{R}))$  where  $k_a$  is the sticking coefficient and  $p$  is the constant partial pressure in the gas phase. Accordingly, in order to respect the detailed balance when reaching thermal equilibrium, the desorption rate takes the form  $w_d(\mathbf{R}) = k_{d,0} n(\mathbf{R}) \exp[\beta U(\mathbf{R})]$  with  $\beta = 1/k_B T$  ( $k_B$  is Boltzmann's constant and  $T$  is the absolute temperature). For diffusion, we admit that a molecule can jump from a site  $\mathbf{R}$  to a site  $\mathbf{R}'$  according to the Metropolis rule

$$w_{\text{diff}}(\mathbf{R}, \mathbf{R}') = \Gamma \quad \text{if } U(\mathbf{R}') < U(\mathbf{R}), \quad (2.3)$$

$$\Gamma \exp[-\beta(U(\mathbf{R}') - U(\mathbf{R}))] \quad \text{if } U(\mathbf{R}') > U(\mathbf{R}), \quad (2.4)$$

which amounts to assuming that the activation energy for hopping is simply the difference between the energy in the final and the initial states.

In order to reduce the master equation to a multivariate Fokker-Planck equation, a coarse graining of the surface must be achieved by dividing it into boxes containing a relatively large number  $Z$  of sites. If the mixing properties are sufficient, the state of each box located at a macroscopic position  $\mathbf{r}$  is entirely determined by a local fluctuating concentration  $c(\mathbf{r}, t)$  defined as the fraction of occupied sites inside a box. Moreover, if  $Z$  is large, this quantity is only slightly modified by the different elementary processes, so that a Kramers-Moyal expansion of the probability  $P[c(\mathbf{r}), t]$  in powers of the inverse number of sites is possible inside each box.<sup>26)</sup> The Fokker-Planck equation obtained in this way [for details, see Ref. 13]) is equivalent to a Langevin-type stochastic differential equation for the coverage, reading in this case

$$\begin{aligned} \frac{\partial c}{\partial t} = & k_a p (1 - c) - k_{d,0} \exp[\beta U(\mathbf{r})] c + D \nabla^2 c + \beta D \nabla [c(1 - c) \nabla U(\mathbf{r})] \\ & + \xi_a(\mathbf{r}, t) + \xi_d(\mathbf{r}, t) + \xi_{\text{diff}}(\mathbf{r}, t), \end{aligned} \quad (2.5)$$

where we have dropped, for simplicity, the explicit space and time dependence for  $c$ . The mesoscopic interaction potential  $U(\mathbf{r})$  is given by  $-\int u(\mathbf{r}' - \mathbf{r}) c(\mathbf{r}') d\mathbf{r}'$ ,

the diffusion coefficient  $D$  is defined as  $\Gamma a^2$  where  $a$  is the lattice constant; all the other parameters have the same meaning as before. The internal noises  $\xi_a(\mathbf{r}, t)$ ,  $\xi_d(\mathbf{r}, t)$  and  $\xi_{\text{diff}}(\mathbf{r}, t)$  take into account fluctuations due to adsorption, desorption and diffusion respectively. This approach is expected to be valid if the size of each box is smaller than the interaction radius, representing the smallest characteristic length in the system. Since the kind of interactions encountered between adsorbed particles usually extend over a few lattice lengths, the mesoscopic approach used here is not always fully justified, and one could rather think of relying on the results of Monte Carlo simulations. We believe however that the mesoscopic level of description allows for a qualitative analytical understanding of the spatiotemporal dynamics, which is rarely the case when simulations are in use. Moreover, Vlachos et al. have recently shown<sup>27),28)</sup> that such a mesoscopic description quantitatively describes the diffusion of interacting particles even if the interaction range is very short (nearest neighbors interactions).

In the macroscopic limit, the noise terms can be neglected and Eq. (2.5) reduces to a deterministic form identical to the evolution law derived using the mean field approximation or by referring to phenomenological arguments.<sup>12)</sup> The specificities of the microscopic level nevertheless reflect themselves at this level of description: the desorption rate and diffusion are functions of the interaction potential. Diffusion in particular is the sum of a traditional Fickian term and a nonlinear term which describes the viscous surface flow of the adsorbate  $A$  in the presence of a force induced by a surface gradient of this particle. The factor  $c(1-c)$  is representative of the fact that the flow of particles  $A$  can only pass through the empty sites on the surface. Note that this reaction-diffusion equation is different both from the Ginzburg-Landau equation for a first-order transition with non-conserved order parameter and from the Cahn-Hilliard equation describing phase transitions with a conserved order parameter.<sup>\*)</sup> The homogeneous equilibrium solution(s) is (are) given by solving

$$k_a p (1 - c_{st}) - k_{d,0} \exp(-\beta u_0 c_{st}) c_{st} = 0. \quad (2.6)$$

For high values of the temperature, this equation admits only one (dilute) equilibrium coverage while beneath a given critical temperature  $T_c = u_0/4k_B$ , a first order transition takes place and dense and a dilute phase with coverages  $c_1$  and  $c_2$  can coexist if  $u_0/k_B T \geq 1/c(1-c)$  with  $c = c_1$  or  $c_2$ .

If a spatially extended system is considered, one expects that inside the parametric region of bistability, any interface separating the two homogeneous steady states will evolve so that the metastable state is invaded by the stable one. Such moving interfaces are governed by the complete reaction-diffusion equation where the diffusion coefficient is present and is expected to play an important role. The numerical integrations reveal that these interfaces are indeed characterized by a precursor and a tail extending over distances comparable to the diffusion length  $L_{\text{diff}} = (D/k_d)^{1/2}$ . Moreover, there is usually a depletion of the adsorbates near the dense phase, which

---

<sup>\*)</sup> The flows induced by adsorption and desorption phenomena do not indeed conserve the total coverage.

acts like a sink emptying the neighboring low density region. On the other hand, standing interfaces are also observed when both states are equistable. If the coverage does not vary significantly within the interaction radius, the condition for equistability reads

$$-u_0 c + k_B T \ln \left( \frac{c}{1-c} \right) - \chi \frac{\partial^2 c}{\partial x^2} = \mu_0 \quad (2.7)$$

with  $u_0 = \int u(\mathbf{r}) d\mathbf{r}$  and does not include the diffusion coefficient  $D$  but rather  $\chi = \frac{1}{2} \int \mathbf{r}^2 u(\mathbf{r}) d\mathbf{r} \approx u_0 r_0^2$  so that one expects the width of the standing interface to scale as the interaction radius  $r_0$ . In contrast to the case of moving fronts, the width of the standing interface is thus expected to be very narrow, i.e. much shorter than the corresponding diffusion length, as confirmed by numerical integrations.

These specificities of the profiles will affect the *spontaneous* nucleation and growth of the stable phase inside the metastable one, which we will discuss now. The dynamics of phase transition usually consists in the spontaneous nucleation and subsequent growth of the stable phase into the metastable one. As demonstrated by integrating the stochastic differential equation (2.5), fluctuations of various sizes are indeed spontaneously created in the system (see Fig. 1); among these, nuclei of a sufficient size\*) start to grow and invade the surface which becomes eventually completely covered by the new phase. The growth of nuclei of the dense phase is influenced by the nonlinear diffusion of the adsorbate and a region of local depletion of the adsorbate around each dense cluster is rapidly formed. As a consequence, two moving interfaces begin to interact at distances much larger than the interaction radius so that the formation of small clusters between the islands of the dense phase is prevented. This slows down the propagation of the interfaces and as a consequence one can expect the transition to be completed only after a long time, in a manner very similar to the Ostwald ripening, which is described at its late stage by the Lifshitz-Slyozov theory. In our case, however, the total mass of adsorbate is not conserved because of the flux of matter induced by adsorption and desorption. The final stage of the phase transition, leading to the fusion of the islands, should here be dictated by interactions between the moving fronts as their relative distance approaches the diffusion length.

Since it is the amplitude of local fluctuations that will allow or not a supercritical nucleus of the stable phase to appear, the properties of the internal noise are of prime importance. The explicit form of the noise terms introduced in Eq. (2.5) is given by

$$\xi_a(\mathbf{r}, t) = \left( \frac{k_a p (1-c)}{Z} \right)^{\frac{1}{2}} f_a(\mathbf{r}, t), \quad (2.8)$$

$$\xi_d(\mathbf{r}, t) = \left( \frac{k_{d,0} c}{Z} \right)^{\frac{1}{2}} \exp[\beta U(\mathbf{r})/2] f_d(\mathbf{r}, t), \quad (2.9)$$

$$\xi_{\text{diff}}(\mathbf{r}, t) = \frac{1}{Z^{1/2}} \nabla \left\{ [2Dc(1-c)]^{1/2} \mathbf{f}(\mathbf{r}, t) \right\}, \quad (2.10)$$

---

\*) The critical nucleus, capable to produce both growing and shrinking domains, is determined by the unstable stationary solution of Eq. (2.7) (with  $c(r) \rightarrow c^*$  for  $r \rightarrow \infty$  where  $c^*$  is the metastable state). Its size only depends thus on the interaction radius  $r_0$  which is usually short for adsorbates.

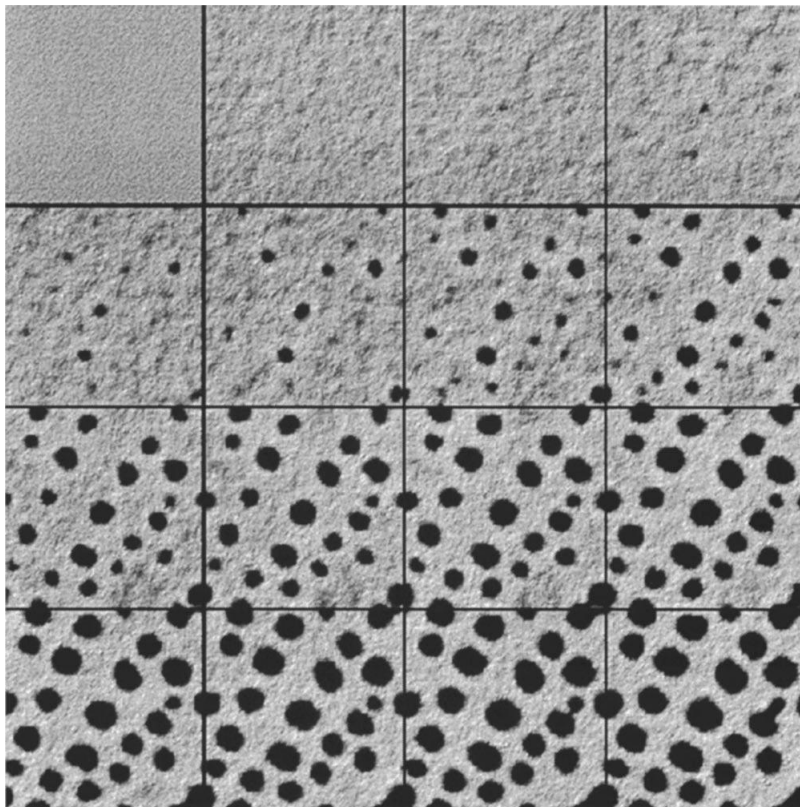


Fig. 1. Numerical simulation of the stochastic equation (2.5) showing the spontaneous nucleation of the dense phase in a 2d system (dark regions correspond to a high coverage). The time interval between the snapshots (from top left to bottom right) is  $5/k_{d,0}$ , while the grid size is  $\Delta x = 0.1(D/k_{d,0})^{1/2}$  and the system linear size is  $L = 16(D/k_{d,0})^{1/2}$ . The other parameters are  $u_0 = 6k_B T$ ,  $k_a p = 0.0753k_{d,0}$ ,  $r_0 = 0.2(D/k_{d,0})^{1/2}$  and  $Z = 2 \cdot 10^3(k_{d,0}/D)$ . Since the simulation of the stochastic equation in 2d requires a large amount of computational time, only the early stage of the transition is depicted here.

with  $f_a$ ,  $f_d$  and  $\mathbf{f}$  being independent white noises of unit intensity and  $Z$  the number of lattice sites per unit area. Obviously, adsorption, desorption and diffusion will not contribute in a similar way to the global noise. All the random forces,  $f_a$ ,  $f_d$  and  $\mathbf{f}$  having the same intensity, it suffices to compare the pre-factors of these stochastic terms to evaluate their respective contribution. Remarkably, they all scale as the inverse of the lattice density  $Z$ , a quantity that is not present in the deterministic evolution laws. The intensity of the noise inside each box is thus inversely proportional to the number of particles contained in it. Despite this similarity, there exist substantial differences between the adsorption-desorption noise and the fluctuations associated with diffusion. The diffusion noise for example is the derivative of a random flux  $\mathbf{j}(\mathbf{r}, t)$  which can be decomposed as a superposition of fluctuating modes with a different wavelength  $l$ :  $\mathbf{j}(\mathbf{r}, t) = \int_0^{+\infty} C_l \phi_l(\mathbf{r}, t)$ . For a characteristic

wavelength, we can estimate that

$$C_l \sim \frac{1}{l Z^{1/2}} [2 D c (1 - c)]^{1/2}. \quad (2.11)$$

On the other hand, the intensity of the adsorption and desorption noises do not depend on the wavelength. For short length scales  $l < L_{\text{diff}}$ , we can thus expect the noise induced by diffusion events to dominate over the ones associated with the other processes; for larger domains the situation is of course reversed. Note also that only the desorption term depends explicitly on the potential interactions, while the noise associated with desorption or diffusion depend on it through the local coverage  $c$ .

The mesoscopic approach used for this simple model involving a single adsorbate can also serve as a basis for the study of more complex surface reaction systems. To understand what sort of behaviors can emerge from the interplay of fluctuating surface reaction kinetics and phase transitions, we will now consider the case of a two-species model of non-equilibrium reaction involving interacting adsorbates.

## 2.2. Non-equilibrium microstructures in a two-species model of surface reaction

We now consider a hypothetical surface chemical reaction involving two species in a non-equilibrium annihilation process<sup>17)</sup>



where the adsorbed species  $U$  and  $V$  occupy different adsorption sites,  $*U$  and  $*V$  respectively.  $V$  is assumed to be strongly chemisorbed so that it cannot diffuse across the surface nor desorb thermally. In comparison,  $U$  is weakly bound to the surface, is thus highly mobile and can easily desorb. We consider moreover that particles  $U$  are strongly attracting each other so that a first-order phase transition similar to what has been discussed before is expected to take place. Attractive interactions between particles  $U$  and  $V$  are also considered, while for the sake of simplicity interactions between two particles  $V$  are from now on neglected.

Starting from the master equation associated with this system, one can derive the fluctuating mesoscopic evolution equations for the coverages  $c_U$  and  $c_V$  in a manner very similar to what has been done for the case of a single adsorbate [see Ref. 17) for details]:

$$\begin{aligned} \frac{\partial c_U}{\partial t} = & k_a^U p_U (1 - c_U) - k_{d,0}^U \exp[\beta W(\mathbf{r}, t)] c_U - k_r c_U c_V + D \nabla^2 c_U \\ & + \beta D \nabla [c_U (1 - c_U) \nabla W(\mathbf{r}, t)] + \xi_U(\mathbf{r}, t), \end{aligned} \quad (2.15)$$

$$\frac{\partial c_V}{\partial t} = k_a^V p_V (1 - c_V) - k_r c_U c_V + \xi_V(\mathbf{r}, t), \quad (2.16)$$

where we have once more omitted, for clarity, the explicit temporal and spatial dependence for the variables. Note that, because of lateral interactions, the diffusion of species  $U$  is nonlinear. In these equations,  $k_a^{U(V)}$  and  $p_{U(V)}$  are, respectively, the

sticking coefficient and the partial pressure of the particle  $U$  ( $V$ );  $D = \Gamma_U a^2$  is the diffusion coefficient of  $U$  ( $\Gamma_U$  is the hopping probability,  $a$  the lattice constant and Metropolis diffusion is assumed) and  $k_r$  the reaction constant. Like in the previous case, the desorption rate for  $U$  depends on the local interaction potential

$$W(\mathbf{r}, t) = - \int w_{UU}(\mathbf{r}' - \mathbf{r}) c_U(\mathbf{r}') d\mathbf{r}' - \int w_{UV}(\mathbf{r}' - \mathbf{r}) c_V(\mathbf{r}') d\mathbf{r}'$$

which is now the sum of all the energetic contributions arising from the pairwise attractive interactions between particles  $U$  and between particles  $U$  and  $V$ . We assume for simplicity that both binary interactions  $w_{UU}$  and  $w_{UV}$  have Gaussian profiles similar to Eq. (2.2) with the same characteristic length  $r_0$  but with different strengths  $w_{UU}^0$  and  $w_{UV}^0$ . The random terms  $\xi_U(\mathbf{r}, t)$  and  $\xi_V(\mathbf{r}, t)$  reflect the intrinsically stochastic nature of the adsorption, desorption, reaction and diffusion processes. They can be expressed as

$$\begin{aligned} \xi_U(\mathbf{r}, t) &= \left( \frac{k_a^U p_U (1 - c_U)}{Z} \right)^{\frac{1}{2}} f_a(\mathbf{r}, t) + \left( \frac{k_{d,0}^U e^{\beta W(\mathbf{r}, t)} c_U}{Z} \right)^{\frac{1}{2}} f_d(\mathbf{r}, t) \\ &\quad + \left( \frac{k_r c_U c_V}{Z} \right)^{\frac{1}{2}} f_r(\mathbf{r}, t) + \frac{1}{Z^{1/2}} \nabla \left\{ (2D c_U (1 - c_U))^{1/2} \right\} \mathbf{f}(\mathbf{r}, t), \\ \xi_V(\mathbf{r}, t) &= \left( \frac{k_a^V p_V (1 - c_V)}{Z} \right)^{\frac{1}{2}} g_a(\mathbf{r}, t) + \left( \frac{k_r c_U c_V}{Z} \right)^{\frac{1}{2}} f_r(\mathbf{r}, t), \end{aligned}$$

with  $Z$  having the same signification as before.

While this model does not correspond to a realistic real-world system, it has the advantage to represent a simple, generic and essentially irreversible example of surface reaction. In this view it is expected to give rise to generic non-equilibrium behaviors, which can be quantified in the deterministic limit. In order to avoid cumbersome notations, we will use from now on the dimensionless parameters  $\alpha = k_a^U p_U / k_{d,0}^U$ ,  $\kappa = k_r / k_a^U p_U$ ,  $\gamma = k_a^V p_V / k_r$ ,  $\varepsilon = \beta w_{UU}^0$ ,  $\varepsilon' = \beta w_{UV}^0$  and  $\rho = r_0 / L_r$ ,  $L_r = (D / k_r)^{1/2}$  being the reactive diffusion length of particles  $U$ . Neglecting thus fluctuations, the homogeneous steady state coverages  $u_0$  and  $v_0$  are found as the solutions of

$$1 - c_U - \alpha^{-1} c_U \exp[-\varepsilon c_U - \varepsilon' c_V (c_U)] - \kappa c_U c_V (c_U) = 0$$

with  $c_V(c_U) = \gamma / (\gamma + c_U)$ . This equation can admit one or three real positive solutions; in the latter case, there is coexistence between a dilute and a dense phase. The stability of these states can be tested by adding inhomogeneous perturbations of the form  $\delta_{U(V)} \exp(ik \mathbf{r} + \omega_k t)$ . Keeping only the linear terms, the problem reduces to finding the eigenvalues  $\omega_k^+$  and  $\omega_k^{-*}$  of the corresponding linearization matrix. Any uniform stationary state is stable as long as all the perturbation modes are decaying with time. As soon as  $\text{Re}(\omega_k^+) = d/dk^2 \text{Re}(\omega_k^+) = 0$  for a given critical

\* The eigenvalue  $\omega_k^+$  being the one with the largest real part.

wavenumber  $k_c$ , an instability characterized by the corresponding wavenumber will begin to grow. In this example, two distinct situations can then be encountered.

First,  $\omega_k$  can be complex at the instability point that can thus be assimilated to a Hopf bifurcation. The wavenumber of the first unstable mode is non-zero, so that the Hopf bifurcation is accompanied by a symmetry breaking in space, i.e. traveling or standing waves should develop. An example of such waves is depicted in Fig. 2. The wavelength of these structures can be easily estimated at the boundaries of the unstable region (where  $u_0 = u_D = (1 \pm \sqrt{1 - 4/\varepsilon})/2$ ) if the interaction radius is much smaller than the characteristic reaction length. Indeed, in such conditions  $\rho_0 = r_0/L_r \ll 1$  and

$$\lambda_w \approx (2\pi^2)^{1/2} \left[ \frac{\gamma}{(1-u_D)(\gamma+u_D)} \right]^{-1/4} \sqrt{r_0 L_r}. \quad (2.17)$$

Since this characteristic length is proportional to  $\sqrt{r_0 L_r}$ , it would generally lie in the submicrometer range for surface chemical reactions.

Second,  $\omega_k^+$  can be real at the instability point. This corresponds to a Turing-like bifurcation and leads to the formation of stationary structures. For small interaction radius, the wavelength of this first unstable mode reads

$$\lambda_T = (2\pi^2)^{1/2} \left[ \frac{\gamma}{(1-u_D)(\gamma+u_D)} - \frac{\gamma u_D}{(\gamma+u_D)^2} \right]^{-1/4} \sqrt{r_0 L_r} \quad (2.18)$$

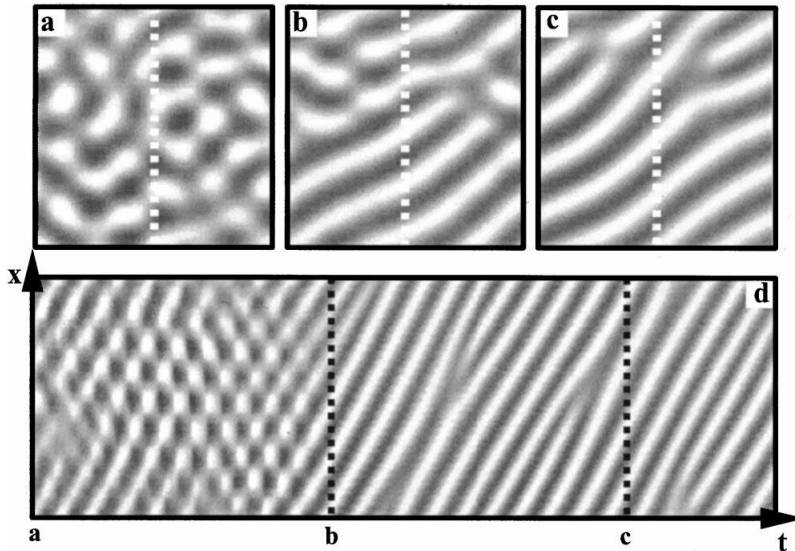


Fig. 2. Travelling patterns obtained by numerical integration of Eqs. (2.15) and (2.16) in 2 dimensions in the absence of noise: the gray scale corresponds to the coverage of  $U$ , with darker areas being higher concentrations. The frames (a), (b) and (c) correspond to times  $t = 18/k_{d,0}^U$ ,  $t = 45/k_{d,0}^U$  and  $t = 72/k_{d,0}^U$  respectively; the figure (d) is the spatiotemporal plot along the vertical dashed line for  $18/k_{d,0}^U < t < 85/k_{d,0}^U$ . The total linear size is  $4.2L_{\text{diff}}$ ,  $\varepsilon = 5$ ,  $\varepsilon' = 3$ ,  $\alpha = 0.5$   $\gamma = 3$  and  $r_0 = 0.07L_{\text{diff}}$ .

and these structures are expected, as before, to belong to the submicrometric domain. It should be noted however that even in the case of a codimension-2 bifurcation, the wavelength of the stationary and the travelling structures remain different: the characteristic size of the stationary microstructures is always larger than that for the travelling waves.

Varying the free parameters, the model, despite its apparent simplicity, proposes a large variety of complex spatiotemporal phenomena as each state can become unstable through one of the aforementioned bifurcations. In the limit where  $\rho \rightarrow 0$ , the end points of the wave bifurcation are approximately given by  $\varepsilon'_{c,w} = \varepsilon \kappa [(\gamma + u_D)^3 + \gamma u_D] / (\gamma k_w^2)$  while for the Turing bifurcation we have  $\varepsilon'_{c,T} = \varepsilon \kappa [(\gamma + u_D)^3 + \gamma u_D] / (\gamma k_T^2)$ . Since  $\varepsilon'_{c,w} < \varepsilon'_{c,T}$ , the two types of instabilities can be found separately or even coexist (see Fig. 3). In the latter case, the choice of initial conditions determines whether stationary or travelling patterns are formed. The selection and the stability of the different patterns in the vicinity of the bifurcations can be determined by a weakly nonlinear analysis, but these topics will not be discussed here.

We rather focus now on the effects of fluctuations, as the patterns that are formed can be of the order of the interaction radius. While we observe, by numerical simulations of Eqs. (2.15) and (2.16), that the formation of Turing structures is usually robust with respect to fluctuations, the effects of noise on the travelling waves are not negligible. In 1 dimension, we observe for example a never ceasing spontaneous nucleation of travelling waves leading to a rather chaotic behavior and

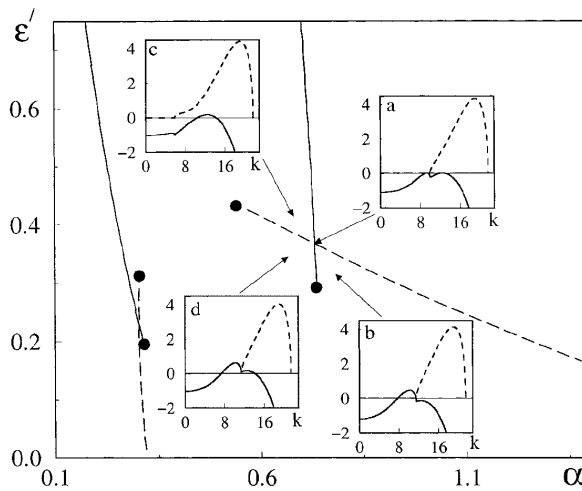


Fig. 3. Bifurcation diagram in the parameter plane  $(\alpha, \varepsilon')$ . The other parameters are  $\varepsilon = 4.2$ ,  $\gamma = 3$ ,  $\kappa = 1$  and  $r_0 = 0.025(D/k_{d,0}^U)^{1/2}$ . The solid line corresponds to the wave bifurcation and the dashed one to the Turing instability. The uniform phase is unstable in the region delimited by the left-most and the right-most of these lines. Dots represent the end points of the bifurcations. The insets display the dispersion relations at the points marked by the arrows; (a)–(d) correspond to  $\alpha = 0.73$  and  $\varepsilon' = 0.368$ ,  $\alpha = 0.78$  and  $\varepsilon' = 0.315$ ,  $\alpha = 0.667$  and  $\varepsilon' = 0.415$ , and  $\alpha = 0.679$  and  $\varepsilon' = 0.346$ , respectively. The bold solid lines in the insets correspond to the real part of the eigenvalues  $\omega_k$ , the dashed lines to their imaginary parts.

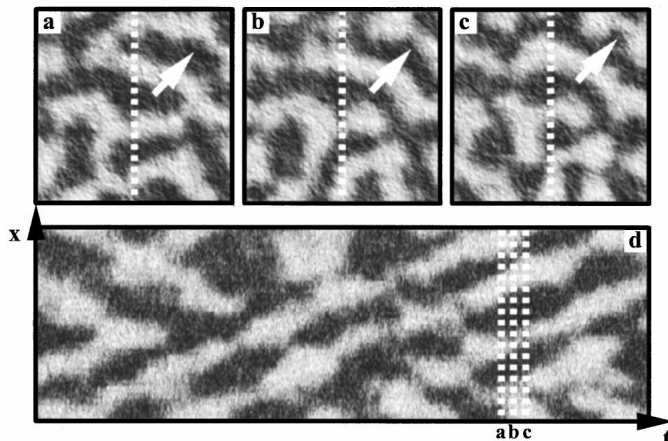


Fig. 4. Travelling wave fragments observed by numerical integration of Eqs. (2.15) and (2.16) including the noise terms with  $Z = 1.07 \cdot 10^5 L_{\text{diff}}^{-2}$ . All the parameters are identical to those of Fig. 2, except for  $\alpha = 0.08$ ,  $L = 1.7L_{\text{diff}}$  and  $r_0 = 0.028L_{\text{diff}}$ . Snapshots (a)–(c) are separated by time intervals  $\Delta t = 0.89/k_{d,0}^U$  while the spatiotemporal plot is the time evolution along the vertical dashed line for  $t = 44.6/k_{d,0}^U$ .

non-harmonic profiles as the different zones begin to interact. In 2d, the individual travelling stripes observed in the deterministic limit are broken in many short travelling fragments (see Fig. 4). Merging and splitting of these fragments are observed as they often collide but, remarkably, despite the fluctuation in their shape, they move with an almost constant velocity.

While the properties of the two models that have been presented here are interesting, it would be desirable to study the dynamics of systems which are known experimentally to lead to nanometric structures. In this view, we will now consider the case of surface reactions involving co-adsorbed nonreactive metallic species.

### §3. Surface reactions with co-adsorbed nonreactive species

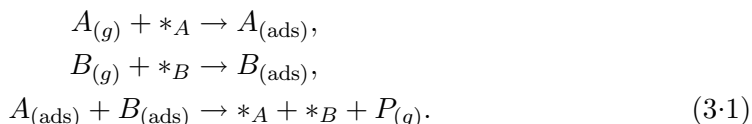
In heterogeneous catalysis, nonreactive species are often found on the surface in addition to the chemicals involved in the reactions. Among these, promoters (or poisons) are of particular interest: they are usually added in small quantities to catalytic systems in order to increase (decrease) the rate of a given reaction.<sup>22)</sup> In the case of heterogeneous catalysis, these particles are believed to be metallic ions irreversibly adsorbed on the surface of the solids where they can rapidly diffuse and locally modify the rate and selectivity of given reactive events. Different microscopic mechanisms, such as variations in the density of metal states at the Fermi level and electrostatic interactions between the promoter and the adsorbates, can be invoked to explain this influence.<sup>22), 29)</sup>

Promoted surface reactions clearly belong to the class of reactive weakly condensed systems involving molecules with lateral energetic interactions, which can lead, as we have seen before, to the emergence of complex phenomena. However, and despite their frequent use in real-world catalysis, the role of such promoting (poi-

soning) species in the formation of spatiotemporal patterns has been only recently studied experimentally. It was shown not long ago that during water formation by the catalytic  $\text{H}_2 + \text{O}_2$  reaction on Rh(110) in the presence of co-adsorbed metal(s), the adsorbates are not always distributed homogeneously on the surface but can spontaneously redistribute. If the co-adsorbed metal is potassium, periodic patterns formed by dense islands comprising K+O are formed<sup>(20), (23)–(25)</sup> while in other cases (gold, palladium) the oxygen and the co-adsorbed metal still form regular structures but separate under reaction conditions.<sup>(30)</sup> In this section, we propose to study an abstract model representative of this class of systems in order to understand the basic mechanism at the origin of such phenomena.<sup>(20), (21)</sup> The typical wavelength of the periodic patterns being of the order of a few to tens of micrometers, we will focus our attention on the deterministic limit of the mesoscopic equations. The implementation of fluctuations will be the object of a future work.

### 3.1. The model

In the reaction scheme considered here, particles  $A$  and  $B$  adsorb from the gas phase onto the catalytic surface, diffuse on it and react to form a product  $P$  that desorbs immediately:



$A_{(\text{ads})}$  and  $B_{(\text{ads})}$  denote adsorbed molecules,  $*A$  and  $*B$  represent vacant surface sites for the molecules  $A$  and  $B$  respectively,<sup>\*)</sup> and  $P$  is the product. The reaction itself is maintained far from thermal equilibrium so that the lifetime of  $P$  on the surface and loss of reactants through desorption can be neglected. We consider in addition to this annihilation process the presence of an adsorbate  $C$  that does not adsorb, desorb nor react but diffuses rapidly on the surface. Being representative of a promoter (poison), we assume that this species modifies locally the reaction rate constant as  $\nu(\mathbf{R}) = \nu_0 \exp[\rho n_C(\mathbf{R})/k_B T]$ , where  $\nu_0$  is the reaction rate constant in the absence of promoter,  $n_C(\mathbf{r})$  is the local occupation number of  $C$  and the coefficient  $\rho$  specifies how strongly the reaction is affected by the promoter. Note that this expression amounts to assuming that  $C$  can increase ( $\rho < 0$ ) or decrease ( $\rho > 0$ ) the activation energy for the reaction, being respectively a poison and a promoter. For simplicity however, the species  $C$  will generally be called promoter, unless the case of the negative  $\rho$  is explicitly considered.

The promoters usually have strong lateral energetic interactions with at least one of the surface reactants. Considering in this example only interactions between  $A$  and  $C$ , two potentials can be defined  $U(\mathbf{R}) = -\sum_{\mathbf{R}'} u_{AC}(\mathbf{R}' - \mathbf{R}) n_C(\mathbf{R}')$ ,  $V(\mathbf{R}) = -\sum_{\mathbf{R}'} u_{AC}(\mathbf{R}' - \mathbf{R}) n_A(\mathbf{R}')$  with  $u_{AC}$  being a Gaussian pairwise interaction potential similar to Eq. (2.2) with intensity  $u_0$  and interaction length  $r_0$ . Lateral interactions between similar particles, the reactants  $A$  and  $B$  and between the promoter  $C$  and

<sup>\*)</sup> It is assumed for simplicity that the adsorption sites for the components  $A$  and  $B$  are different on the surface.

the reactant  $B$  are absent for the sake of simplicity. Like before, Langmuir adsorption is considered and the hopping probability of  $A$  and  $C$  is assumed to depend on the potentials  $U$  and  $V$  respectively via the Metropolis rule.

In view of the wavelength of patterns found in experiments, we will focus our attention on the deterministic limit of the evolution equations. Taking into account the aforementioned hypotheses, the evolution laws for the coverages (which will be denoted as  $\theta_{A,B,C}$ ) can be cast into the form

$$\begin{aligned} \dot{\theta}_A = & P_A (1 - \theta_A) - \nu_0 e^{w\theta_C} \theta_A \theta_B + D_A \nabla^2 \theta_A \\ & + \beta D_A \nabla [\theta_A (1 - \theta_A) \nabla U(\mathbf{r})], \end{aligned} \quad (3.2)$$

$$\dot{\theta}_B = P_B (1 - \theta_B) - \nu_0 e^{w\theta_C} \theta_A \theta_B + D_B \nabla^2 \theta_B, \quad (3.3)$$

$$\dot{\theta}_C = D_C \nabla^2 \theta_C + \beta D_C \nabla [\theta_C (1 - \theta_C) \nabla V(\mathbf{r})], \quad (3.4)$$

where  $U(\mathbf{r}) = -\int d\mathbf{r}' w_{AC}(\mathbf{r}' - \mathbf{r}) \theta_C(\mathbf{r}')$ ,  $V(\mathbf{r}) = -\int d\mathbf{r}' w_{AC}(\mathbf{r}' - \mathbf{r}) \theta_A(\mathbf{r}')$ ,  $P_A = k_a^A p_A$ ,  $P_B = k_a^B p_B$  and  $w = \rho/k_B T$ . The diffusion coefficients are  $D_A = \Gamma_A a^2$  and  $D_C = \Gamma_C a^2$  with  $\Gamma_A$ ,  $\Gamma_C$  and  $a$  being the hopping probabilities of  $A$ ,  $C$  and the lattice constant respectively.

These evolution equations have a uniform stationary state where all coverages are constant:  $\theta_A(\mathbf{r}) \equiv a$ ,  $\theta_B(\mathbf{r}) \equiv b$ , and  $\theta_C(\mathbf{r}) \equiv c$ . The coverage  $c$  in the uniform state is determined by the initial conditions and can be considered as a parameter of the system. The uniform coverages  $a$  and  $b$  of both reactants are determined by a balance between adsorption and reaction:

$$\begin{aligned} a = & \frac{P_A}{P_A + \nu_0 e^{w c} b}, \\ b = & -\frac{P_A P_B + \nu_0 e^{w c} (P_A - P_B)}{2 \nu_0 e^{w c} P_B} \\ & \pm \frac{\left[ (P_A P_B + \nu_0 e^{w c} (P_A - P_B))^2 + 4 \nu_0 e^{w c} P_A P_B^2 \right]^{\frac{1}{2}}}{2 \nu_0 e^{w c} P_B}, \end{aligned}$$

where only one positive solution exists. We will now consider analytically the spatial instability of this uniform state with respect to small spatiotemporal perturbations. Pattern formation taking into account the nonlinear contributions to the dynamics will be studied numerically in the following section.

### 3.2. Linear stability analysis

Because of the coupling between energetic interactions, diffusion of adsorbed species and chemical reaction, the uniform stationary state of the system can become unstable with respect to the growth of nonuniform perturbations. To investigate the stability of the uniform state  $(a, b, c)$ , we introduce small variations in the coverages of the form  $\theta_X(\mathbf{r}, t) = x + \delta_X \exp(i\mathbf{k}\mathbf{r} + \omega_k t)$  for each species. Keeping only the leading terms (of the order of  $\delta_A, \delta_B, \delta_C$ ), the growth rates of the various spatial

modes are given by the eigenvalues of the linearization matrix  $\mathcal{L}(k) =$

$$\begin{pmatrix} -P_A - \nu_0 b e^{w c} & -\nu_0 a e^{w c} & \varepsilon D_A a (1 - a) k^2 e^{(-r_0^2 k^2/4)} \\ -D_A k^2 & & -\nu_0 a b w e^{w c} \\ -\nu_0 b e^{w c} & -P_B - \nu_0 a e^{w c} & -\nu_0 a b w e^{w c} \\ & -D_B k^2 & \\ \varepsilon D_C c (1 - c) k^2 e^{(-r_0^2 k^2/4)} & 0 & -D_C k^2 \end{pmatrix}, \tag{3.5}$$

where  $\varepsilon = u_0/k_B T$ . Numerical investigations of the considered model show that it does not exhibit oscillations and therefore, when an instability of the uniform state occurs, it corresponds to a Turing-like bifurcation characterized by an unstable mode with a purely real  $\omega_k$ . The instability boundary is determined by the condition that  $\omega_{k_c} = (d\omega_k/dk)_{k_c} = 0$ , or equivalently that

$$\text{Det}(\mathcal{L}(k_c^2)) = \left( \frac{d}{dk^2} \text{Det}(\mathcal{L}(k^2)) \right)_{k_c^2} = 0. \tag{3.6}$$

These requirements lead to the following system of equations (we assume  $k_c \neq 0$ ):

$$D_A D_B (1 - \delta e^{-r_0^2 k_c^2/2}) k_c^4 + \left[ \sigma - D_A (P_B + \nu_0 e^{w c} a) \delta e^{-r_0^2 k_c^2/2} + D_B \phi e^{-r_0^2 k_c^2/4} \right] k_c^2 + \mu + P_B \phi e^{-r_0^2 k_c^2/4} = 0, \tag{3.7}$$

$$\begin{aligned} & \left[ \frac{r_0^2}{2} D_A D_B \delta e^{-r_0^2 k_c^2/2} \right] k_c^6 + \left[ \frac{r_0^2}{2} D_A (P_B + \nu_0 e^{w c} a) \delta e^{-r_0^2 k_c^2/2} \right. \\ & \left. + 3 D_A D_B (1 - \delta e^{-r_0^2 k_c^2/2}) - \frac{r_0^2}{4} D_B \phi e^{-r_0^2 k_c^2/4} \right] k_c^4 \\ & + \left[ 2 \sigma - 2 D_A (P_B + \nu_0 e^{w c} a) \delta e^{-r_0^2 k_c^2/2} + 2 D_B \phi e^{-r_0^2 k_c^2/4} \right. \\ & \left. - \frac{r_0^2}{4} P_B \phi e^{-r_0^2 k_c^2/4} \right] k_c^2 + \mu + P_B \phi e^{-r_0^2 k_c^2/4} = 0. \end{aligned} \tag{3.8}$$

Here, new notations have been introduced:

$$\begin{aligned} \delta &= \varepsilon^2 a (1 - a) c (1 - c), \\ \mu &= P_A \nu_0 e^{w c} a + P_B \nu_0 e^{w c} b + P_A P_B, \\ \sigma &= P_A D_B + \nu_0 e^{w c} b D_B + P_B D_A + \nu_0 e^{w c} a D_A, \\ \phi &= \varepsilon a b w e^{w c} c (1 - c). \end{aligned} \tag{3.9}$$

To solve Eqs. (3.7) and (3.8), we first take into account that the interaction radius  $r_0$  is a natural small parameter for the systems under consideration, so that  $\exp(-r_0^2 k_c^2/2) \approx \exp(-r_0^2 k_c^2/4) \approx 1$ . Since both expressions are then polynomials,

it suffices then to express  $\delta$  from the first of them

$$\delta = \frac{D_A D_B k_c^4 + (\sigma + D_B \phi) k_c^2 + \mu + P_B \phi}{D_A D_B k_c^4 + D_A (P_B + \nu_0 e^{w c} a) k_c^2} \quad (3.10)$$

and substitute this into Eq. (3.8). An approximate solution of the quartic equation for  $k_c^2$  derived in this way can be found by taking into account once again that the interaction radius  $r_0$  is usually very small. Keeping only the leading terms, this equation is easily solved and the wave number of the critical mode is determined:

$$k_c^2 \approx \frac{1}{r_0} \left[ \frac{2(P_A + \nu_0 e^{w c} b + \varepsilon a b \nu_0 w e^{w c} c(1 - c))}{D_A} \right]^{1/2} \quad (3.11)$$

corresponding to a critical wavelength

$$\lambda_c \approx 2\pi \sqrt{r_0 L_{\text{kin}}} \quad (3.12)$$

with the “kinetic length” being

$$L_{\text{kin}} = \sqrt{\frac{D_A}{2(P_A + \nu_0 e^{w c} b + \varepsilon a b \nu_0 w e^{w c} c(1 - c))}}. \quad (3.13)$$

Analyzing these results, we first notice that in accordance with the simplest models in the previous section, the wavelength of patterns emerging at the criticality lies somewhere between the interaction radius  $r_0$  and some length scale depending on the kinetic parameters. This suggests that the periodicity of such stationary patterns depends on the specificities of the considered system (through the interaction radius, the strength of interaction or diffusion coefficients) but can be directly controlled through external parameters such as the pressures of reactants or the temperature, even if the dependence of  $\lambda_c$  in these quantities is already here quite complex. Note that the wave number of the critical mode (and thus the critical wavelength) does not depend on the diffusion constants of the species  $B$  and  $C$ . While the independence with respect to  $D_B$  is expected to remain valid only for small  $r_0$  and near the criticality, this is not the case for the promoter for which this result is general and is not sensitive to a particular approximation.

Substituting the critical wave number into Eq. (3.10), using the definition of  $\delta$  and keeping again only the leading term in the interaction radius  $r_0$ , we find that the instability boundary is approximately determined by the condition

$$\varepsilon_c^2 \approx \frac{1}{a(1 - a)c(1 - c)}. \quad (3.14)$$

This instability boundary is effectively the same as the boundary for spinodal decomposition in the mixture of two species  $A$  and  $C$  with surface coverages  $a$  and  $c$  in absence of reaction. Since only the square of  $\varepsilon$  enters into the condition (3.14) we expect the emergence of an instability both for attraction ( $\varepsilon > 0$ ) and repulsion ( $\varepsilon < 0$ ) between species  $A$  and  $C$ . This condition leads, as we will now show, to the formation of patterns qualitatively similar to those observed in experiments.

### 3.3. Numerical simulations

Numerical simulations of Eqs. (3·2)–(3·4) have been performed in order to verify the predictions of the linear stability analysis and to study the nonlinear behavior of the system. Because of the rapid exponential decrease of the interaction potential the interaction function (2·2) was truncated at distances exceeding  $2r_0/\Delta x$  to speed up simulations. Periodic boundary conditions were used and a gray scale is considered for the coverages, where higher concentrations appear brighter. As initial conditions, the unstable stationary uniform state of the system  $\theta_A = a$ ,  $\theta_B = b$  and  $\theta_C = c$  with small local random perturbations of about one percent in magnitude was always chosen.

Numerical simulations for the simpler case  $w = 0$ , where the coadsorbed species  $C$  does not modify the reaction rate constant, will be first presented. Figure 5 shows an example of an evolution starting with a randomly performed uniform state. In this space-time diagram, time runs along the horizontal axis and the spatial coordinate of the simulated one-dimensional system is varied along the vertical axis. We see that the uniform state is indeed unstable and a stationary periodic pattern develops, as predicted by the linear stability analysis. Figure 6(a) displays profiles of all three coverages in such a pattern at the steady state. Since the parameters are close to the instability boundary, the amplitudes of spatial variation are relatively small here and the pattern is approximately harmonical. The local coverage of the reactant  $A$  follows the variation of the surface concentration of species  $C$  because of attractive interactions while the coverage of reactant  $B$  exhibits weak antiphase variation (it is rapidly consumed in  $A$ -rich regions).

In Fig. 6(b), the interaction strength is increased to  $\varepsilon = 20$ , as compared with  $\varepsilon = 5$  in Fig. 6(a). The concentration profiles are in this case strongly unharmonical and a periodic pattern of domains with sharp interfaces is clearly observed. Inside each domain, the coverage of species  $C$  reaches its maximum possible level of unity and the surface concentration of the reactant  $A$  is strongly increased. Outside of the domains, almost no species  $C$  is found and the coverage of  $A$  is very small. This situation is strongly similar to what is observed in the experiments in the case of attractive interactions between the promoter and oxygen (in the case of coadsorbed K). Nonlinear pattern formation has also been observed numerically in two-dimensional systems, but will not be illustrated here. Starting from a randomly perturbed uniform state, the system develops a spatial pattern representing an array of dots or elongated islands. These regions are characterized by local increases of the coverages of species  $A$  and  $C$ . Note that the wavelength of the pattern seen in numerical simulations and the numerical values of critical parameters (in 1 and 2 dimensions) agree with the approximate analytical predictions (3·11) and (3·14) yielded by the linear stability analysis within a few percent even for relatively large values of  $r_0 \approx 0.5$ .

As predicted by the analysis, the instability of the uniform state is also found in numerical simulations in the case of repulsive interactions ( $\varepsilon < 0$ ). Figures 7(a) and (b) display spatial profiles of all three species in the asymptotic stationary periodic patterns for relatively weak and strong repulsive interactions. The main

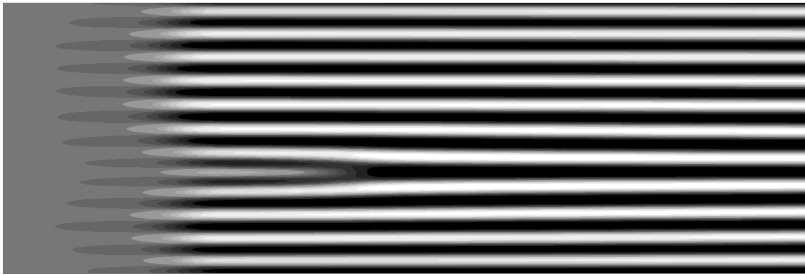


Fig. 5. Space-time diagram showing the development of a periodic spatial pattern in the coverage of species  $C$ . Time runs along the horizontal axis, spatial coordinate is plotted along the vertical axis. The size of the one-dimensional system is  $L = 20$  and the displayed time interval is  $T = 50$ . The model parameters are  $P_A = P_B = D_A = D_B = D_C = 1$ ,  $c = 0.5$ ,  $\varepsilon = 5$ ,  $r_0 = 0.2$ ,  $\nu_0 = 1$  and  $w = 0$ .

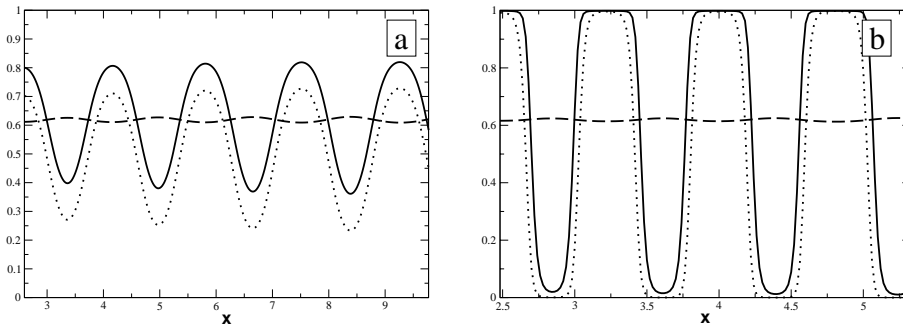


Fig. 6. Stationary distribution profiles for species  $A$  (bold curve),  $B$  (dashed line) and  $C$  (dots) in a one-dimensional system in the case of attractive interactions with (a)  $\varepsilon = 5$  and (b)  $\varepsilon = 20$ . Other parameters are the same as in Fig. 5. Only part of the system with total size  $L = 20$  is shown.

difference with Fig. 6 for attractive interactions is that now species  $A$  and  $C$  tend to avoid each other. The spatial segregation is almost complete in the case of strong repulsion [Fig. 7(b)] which is closed to what is observed experimentally in the case of co-adsorbed Au and Pd.

All the results presented so far were obtained by assuming that  $C$  has no direct effect of promotion or poisoning. When  $w \neq 0$ , this species becomes effectively a promoter or a poison, which can affect strongly the pattern formation. Figure 8(a) shows spatial distributions of reactants and promoter in the periodic stationary pattern in the case of attractive interactions. The increased reaction rate inside mixed promoter-reactant domains leads to a decrease in the amplitude of the periodic pattern because of fast consumption of  $A$ . In contrast to this, the amplitude is increased if species  $C$  is a poison [Fig. 8(b)]. If poisoning is sufficiently strong, the coverage of the second reactant  $B$  becomes also increased inside the domains, as can already be seen in Fig. 8(b). If  $A$  and  $C$  repel each other, similar effects are observed: in the case of promotion, the reaction is most efficient in the domains filled with  $C$ , thus leading to dense domains with stiff boundaries. In the case of poisoning, the reaction is very weak inside the domains filled with  $C$ , which leads to a small increase

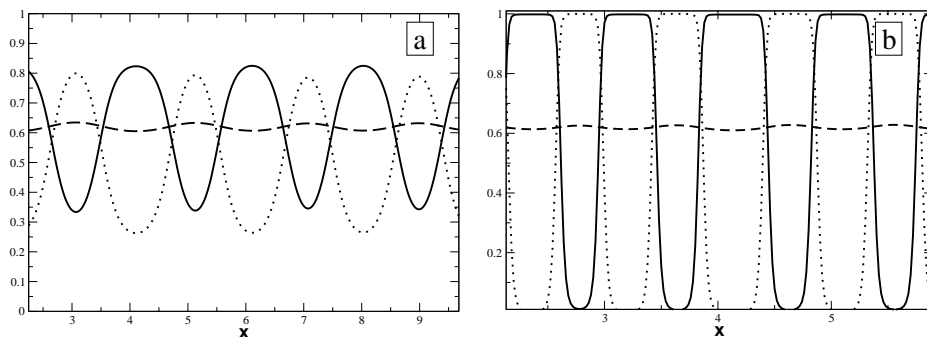


Fig. 7. Stationary distribution profiles for species *A* (bold curve), *B* (dashed line) and *C* (dots) in a one-dimensional system in the case of repulsive interactions with (a)  $\varepsilon = -5$  and (b)  $\varepsilon = -20$ . Other parameters are the same as in Fig. 5.

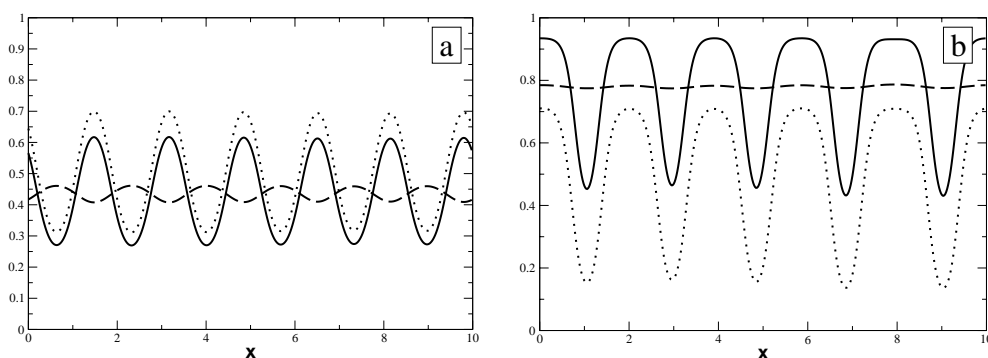


Fig. 8. Stationary distribution profiles for species *A* (bold curve), *B* (dashed line) and *C* (dots) in a one-dimensional system (a) with a promoter ( $w = 2$ ) and (b) with a poison ( $w = -2$ ). Other parameters are the same as in Fig. 5.

of the coverage of *A* in these areas and thus to a decreased amplitude of the coverage variation.

In each case, the compartmentalization of the adsorbed species can significantly influence the global reactivity of the surface. To characterize this effect, we have numerically determined the actual reaction rate  $R$  per unit surface area under compartmentalization conditions and compared it with the computed reaction rate  $R_0$  per unit area, assuming uniform distributions of all species. The quantity  $\Delta R = (R - R_0)/R_0$  was then used to characterize the influence of compartmentalization. Even when  $w = 0$ , so that species *C* is neither a promoter nor a poison, the formation of a periodic pattern has some effect on the reactivity. However, this effect is weak under such conditions and only a decrease of  $\Delta R$  by a few percents can be observed. The effect becomes much more pronounced when *C* is a promoter. Figure 9 shows the dependence of  $\Delta R$  on the strength  $\varepsilon$  of attractive interactions in this situation. We see that the reactivity is substantially enhanced as  $\varepsilon$  grows and compartmentalization occurs. The maximum observed increase of the surface reactivity is about 25%. This increase can be attributed to the spontaneous formation of dense *A+C* clusters acting as microreactors where the reaction rate is especially

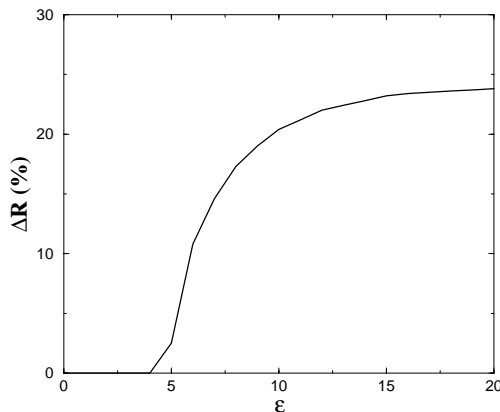


Fig. 9. Growth of the relative global reaction rate under increase of the strength of attractive interactions for promoter with  $w = 2$ . Other parameter and system size are the same as in Fig. 5.

high. When  $C$  is a poison, comparable effects are observed. The global reaction rate is even lower than predicted in the homogeneous limit if  $A$  and  $C$  attract each other, since most  $A$  particles are then captured in dots with a high level of poison. If the interactions are repulsive, the global reaction rate is always smaller than its value without poisoning but can nevertheless become larger than predicted by the homogeneous evolution laws because adsorbate  $A$  is then principally located inside the domains which are poor in the poisoning species.

In the simulations, which we have so far shown, diffusion constants of all species were chosen equal ( $D_A = D_B = D_C = 1$ ). Despite this, periodic patterns of surface concentrations have been found. This clearly indicates that such patterns are different in their origin from the Turing patterns, where a sufficiently strong difference of diffusion constants is always required. We have also performed some simulations where the diffusion constants were varied. In accordance with the predictions of the linear stability analysis, it was observed that changes in the promoter diffusion constant  $D_C$  do not affect the final stationary pattern and only influence the transient process, which becomes longer when diffusion of species  $C$  is slow. We have also checked that spontaneous pattern formation is possible even at small promoter (or poison) concentrations  $c$ , if energetic interactions are strong enough, which is close to the experimental situation. In such cases, very dense domains with stiff boundaries are formed.

#### §4. Metropolis vs Arrhenius diffusion

From the different reaction schemes investigated in the previous sections, we can conclude that the emergence of complex spatial patterns is highly sensitive to the nonlinear diffusion of particles induced by lateral interactions. For the sake of illustration, a very simple mechanism has been here considered (the Metropolis-Kawasaki model) for which the probability of hopping between nearest neighbors depends only

on the energetic level of the particle in its initial and final stage. However, when enlarging the present theory to model realistic situations, one should take into account that there are signs that the mechanism of diffusion of adsorbates should be seen more as an activated process. In this case, the local hopping probability of adsorbates should follow an Arrhenius-like law of the type  $\Gamma(\mathbf{R}) \sim \exp(-\beta \Delta U(\mathbf{R}))$  where  $\Delta U(\mathbf{R})$  is the energy difference between the activated state and the initial state of the diffusing particle. It is legitimate to wonder how the mesoscopic equations for the coverages read in the case of Arrhenius diffusion, and how this could affect the global trends highlighted by the previous studies. To illustrate such modifications, we will consider explicitly the problem of promoted surface reactions studied in the previous section.

The differences between Metropolis and Arrhenius diffusion mechanisms have been recently addressed by Vlachos et al.<sup>27),28)</sup> Starting from the master equation, they derived an evolution law for the local occupation probability from which a mesoscopic diffusion equation can be extracted in the limit of long-range interactions between uncorrelated particles. Their principal conclusion is that while a Metropolis algorithm gives birth to a diffusion coefficient which is essentially constant, an Arrhenius hopping results in  $D(\mathbf{r}) = D^0 e^{\beta U(\mathbf{r})}$  where  $U(\mathbf{r})$  is the interaction potential to which the diffusing particle is subjected. For the monomer-monomer model of promoted reaction considered in §3, the evolution equations (3.2)–(3.4) for the coverages become then

$$\begin{aligned} \dot{\theta}_A = & P_A (1 - \theta_A) - \nu_0 e^{w\theta_C} \theta_A \theta_B + D_A^0 \nabla \left[ e^{\beta U(\mathbf{r})} \nabla \theta_A \right] \\ & + \beta D_A^0 \nabla \left[ e^{\beta U(\mathbf{r})} \theta_A (1 - \theta_A) \nabla U(\mathbf{r}) \right], \end{aligned} \quad (4.1)$$

$$\dot{\theta}_B = P_B (1 - \theta_B) - \nu_0 e^{w\theta_C} \theta_A \theta_B + D_B \nabla^2 \theta_B, \quad (4.2)$$

$$\dot{\theta}_C = D_C^0 \nabla \left[ e^{\beta V(\mathbf{r})} \nabla \theta_C \right] + \beta D_C^0 \nabla \left[ e^{\beta V(\mathbf{r})} \theta_C (1 - \theta_C) \nabla V(\mathbf{r}) \right], \quad (4.3)$$

where all the parameters have the same meaning as before.

Obviously, the linear stability of the (unchanged) homogeneous steady state  $(a, b, c)$  with respect to spatiotemporal perturbations is modified due to the dependence of the diffusion coefficients  $D_A, D_C$  in the local coverages. In fact, performing the same analysis as was done in §3.2, one readily finds that the linearization matrix has exactly the same form but with  $D_A$  and  $D_C$  replaced respectively by  $D_A^0 \exp(-u_0 c)$  and  $D_C^0 \exp(-u_0 a)$ . This should be a general result as far as linear stability analysis is concerned since all the other contributions related to the coverage dependence of the diffusion coefficients result in nonlinear terms. As a consequence, a Turing bifurcation is still found for the model of promoted reaction when  $\varepsilon_c^2 \approx 1/(a(1-a)c(1-c))$ , with a critical wavelength  $\lambda_c \approx 2\pi \sqrt{r_0 L_{\text{kin}}^{\text{Arr}}}$  but where the kinetic diffusion length is now

$$L_{\text{kin}}^{\text{Arr}} = \sqrt{\frac{D_A e^{-u_0 c}}{2(P_A + \nu_0 e^{w c} b + \varepsilon a b \nu_0 w e^{w c} c(1-c))}}. \quad (4.4)$$

Following this analysis, we can conclude that the localization of the bifurcation point

is not modified by the different diffusion mechanism (at least when  $r_0 \ll 1$ ) but that, in opposition to the case of Metropolis diffusion, the periodicity of the patterns that are formed depends strongly (exponentially) in the interaction potential. More specifically, when  $w = 0$ , the critical wavelength is insensitive to the sign of the interaction strength  $u_0$  for Metropolis diffusion, while for an Arrhenius dependence patterns formed in the case of repulsive interactions are larger than those formed when attraction is present.

All these trends were confirmed by numerical integrations of Eqs. (4.1)–(4.3). In Figs. 10(a) and (b) for example, patterns are shown for the specific case  $w = 0$  for Metropolis and Arrhenius dynamics with attractive and repulsive interactions respectively. One can observe that the wavelength in Arrhenius diffusion is indeed shorter than the one with Metropolis diffusion when attractions are considered [Fig. 10(a)] while the situation is reversed when considering repulsion [Fig. 10(b)]. The simulations can also help to illustrate an interesting difference between the two types of diffusion mechanisms far from the bifurcation point. Since the coverages vary periodically in space following the Turing bifurcation, we expect the mobility of the adsorbates to do so. For Metropolis diffusion, the mobility is proportional to  $D\theta(1-\theta)$  while in the case of Arrhenius diffusion, it scales as  $D^0\theta(1-\theta)\exp(\beta U)$ . The ratio between these coefficients is so that in the case of attractive (repulsive) interactions the mobility of a particle following Arrhenius diffusion is lower (greater) than one undergoing a Metropolis rule. As a consequence, far from the bifurcation point, where the interaction potentials can take high values, the effective mobility of particles in the Arrhenius regime can become very low (almost zero) in the regions corresponding to dense clusters. This opens the question whether a mesoscopic approach based on the definition of well-mixed boxes on the surface is still valid in this case.

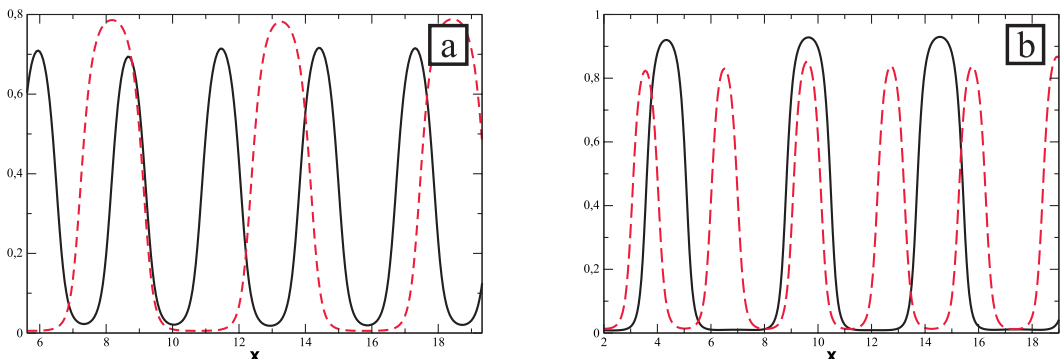


Fig. 10. Stationary coverage for the promoter  $C$  in the of Arrhenius diffusion (plain lines) and Metropolis diffusion (dashed curves). For the two figures,  $P_A = 0.2$ ,  $P_B = 0.1$ ,  $c = 0.3$ ,  $r_0 = 0.5$ ,  $\nu_0 = 1$  and  $w = 0$ . In (a),  $D_A = D_A^0 = D_B = D_B^0 = D_C = D_C^0 = 10$  and  $\varepsilon = 8$ , while in (b),  $D_A = D_A^0 = D_B = D_B^0 = D_C = D_C^0 = 1$  and  $\varepsilon = -8$ . Only a part of the total system (whose size is 50) is shown here.

## §5. Discussion

Pattern formation and complex phenomena are more the rule than the exception in surface chemical reactions. The early experimental observations revealed spatiotemporal dynamics at the order of tens or thousands of micrometers, in other words processes that take place on macroscopic scales with respect to the lattice constant(s) or the diffusion length(s). Due to the emergence of more and more efficient experimental techniques, the submicroscopic details of these systems are however now accessible and specific, complex phenomena have already been identified at this level.

From a theoretical point of view, describing the dynamics at such scales necessitates in general approaches which are more sophisticated than the usual reaction-diffusion equations. The approach used here consists in starting from the master equation describing the evolution of the probability of surface configurations, which is based in the sole assumption that the elementary steps are Markovian processes, and from which a stochastic evolution equation can be for the variables of composition, being in this approach fluctuating quantities. This level of description allows for the inclusion of spontaneous internal fluctuations but also for a clear connection between the atomistic mechanisms of elementary events in the presence of energetic interactions and the corresponding macroscopic limit. The validity of this approach is *a priori* limited by the existence of sufficiently large domains into which the mixing properties are sufficient to consider constant coverages. This supposes that the interactions extend over distances that are large compared with the lattice constants, which could not be the case in several surface systems. However, it provides an analytical understanding of the system and recent results suggest moreover that the domain of validity of such a mesoscopic approach is larger than expected in first view.

On the basis of this approach, different situations have been considered which are representative of elementary surface processes involving strongly interacting particles. In the case of a single interacting adsorbate, phase separation is observed under appropriate conditions and leads to the coexistence of a dense and a dilute state for the coverage. Interestingly, the width and the profile of phases boundaries can be related directly to the parameters of the system: in particular, the width of standing interfaces depends only on the interaction length and is thus much shorter than the diffusion length of the adsorbate. The process of nucleation and growth leading to the coexistence of the two phases is dictated by fluctuations, whose statistical properties can be inferred directly from the parameters of the system thanks to the mesoscopic approach. For more intricate schemes, including chemical reactions, nanometric patterns can be formed under reaction conditions thanks to the combination of short-ranged energetic interactions, reactions and molecular diffusion. Using a simple annihilation scheme between two reactants, stationary and travelling structures are found whose size lies between the interaction radius and the (reactive) diffusion length, in other words in the domain of the nanometer. When such small structures appear, the role of fluctuations can of course become important; it is particularly the case for travelling waves which decompose into merging and splitting

fragments which travel nevertheless with a constant velocity.

Experimentally, promoted (or poisoned) surface reactions provide a large class of important catalytic processes involving particles with strong lateral interactions. Using a simple model, we have shown that in general promoting or poisoning species can destabilize the uniform state of surface reactions and lead to the development of a stationary periodic pattern. The observed structures represent arrays of dense clusters comprising the promoter (or poison) and/or one of the reactants. If interactions are strong, the surface is compartmentalized into self-organized microreactors, which can affect dramatically the surface reactivity. Finally, we have also discussed how the pattern formation detected in the previous sections could be affected by the microscopic details of the diffusion mechanism. More specifically, it was shown that an activated diffusion (Arrhenius mechanism) can result in a coverage-dependent diffusion coefficient modifying thus the wavelength of emerging patterns. Depending on the intensity and the sign of pairwise interactions, the characteristic wavelength of the patterns can become in this case larger (if there is repulsion) or shorter (in the case of attraction) than what is predicted assuming a Metropolis-Kawasaki rule for hopping events.

As a conclusion, the mesoscopic approach used here allows one to identify complex phenomena arising because of the interplay between energetic interactions, nonequilibrium reactions and nonlinear diffusion and to assess the role of fluctuations in these processes. These results open the door to the control of self-organization in the case of surface reactions. Catalytic reactions on microstructured surfaces, prefabricated using microlithography, have already been experimentally studied. The principal result of our theoretical investigation is that the surface can also undergo spontaneous microstructuring through spatial redistribution of adsorbed atoms. In contrast to prefabricated patterns, such microstructures are however flexible: they disappear when the reaction is switched off and their properties can vary, adjusting to the reaction conditions. Taking into account that compartmentalization has a strong effect on the reaction rate, we note that non-equilibrium self-organization phenomena open a way to the construction of *adaptable* catalysts. Depending on the reaction parameters and external controls, such systems would be able to change their structure through redistribution of adsorbed metal atoms. Potentially, both reactivity and selectivity of a catalyst can thus be affected. One could in addition imagine to prepare such structured surface under reaction conditions at high temperatures and “freeze” the system by cooling rapidly and in this way construct surfaces with a well-defined structure. The wavelength of such patterns, being controlled by non-equilibrium reaction constraints, could extend from a few nanometers to tens of micrometers.

In the future, theoretical investigations should be extended to realistic models of various chemical reactions, especially for the promising case of promoted systems. Moreover, kinetic Monte Carlo simulations of such systems could also be performed, in order to clarify the limit of validity of the present mesoscopic description.

## References

- 1) S. Jakubith, H. H. Rotermund, W. Engel, A. von Oertzen and G. Ertl, *Phys. Rev. Lett.* **65** (1990), 3013.
- 2) R. Imbihl and G. Ertl, *Chem. Rev.* **95** (1995), 697.
- 3) T. Zambelli, J. V. Barth, J. Wintterlin and G. Ertl, *Nature* **390** (1997), 495.
- 4) C. Sachs, M. Hildebrand, S. Völkening, J. Wintterlin and G. Ertl, *Science* **293** (2001), 1635.
- 5) T. Visart de Bocarmé and N. Kruse, *Chaos* **12** (2002), 118.
- 6) A. S. Mikhailov and G. Ertl, *Science* **272** (1996), 1596.
- 7) S. C. Glotzer, E. A. Di Marzio and M. Muthukumar, *Phys. Rev. Lett.* **74** (1995), 2034.
- 8) Q. Tran-Cong and A. Harada, *Phys. Rev. Lett.* **76** (1996), 1162.
- 9) M. Motoyama and T. Ohta, *J. Phys. Soc. Jpn.* **66** (1997), 2715.
- 10) T. L. Einstein and J. R. Schrieffer, *Phys. Rev. B* **7** (1973), 3629.  
T. L. Einstein, *CRC Crit. Rev. Solid St. Mater. Sci.* **7** (1978), 261.
- 11) K. H. Lau and W. Kohn, *Surf. Sci.* **75** (1978), 69.
- 12) A. S. Mikhailov and G. Ertl, *Chem. Phys. Lett.* **238** (1995), 104.
- 13) M. Hildebrand and A. S. Mikhailov, *J. Phys. Chem.* **100** (1996), 19089.
- 14) M. Hildebrand, A. S. Mikhailov and G. Ertl, *Phys. Rev. E* **58** (1998), 5483.
- 15) M. Hildebrand, A. S. Mikhailov and G. Ertl, *Phys. Rev. Lett.* **81** (1998), 2602.
- 16) M. Hildebrand, M. Kuperman, H. Wio, A. S. Mikhailov and G. Ertl, *Phys. Rev. Lett.* **83** (1999), 1475.
- 17) M. Hildebrand and A. S. Mikhailov, *J. Stat. Phys.* **101** (2000), 599.
- 18) M. Hildebrand, M. Ipsen, A. S. Mikhailov and G. Ertl, *New J. Phys.* **5** (2003), 61.
- 19) M. Hildebrand, *Chaos* **12** (2002), 144.
- 20) Y. De Decker, H. Marbach, M. Hinz, S. Günther, M. Kiskinova, A. S. Mikhailov and R. Imbihl, *Phys. Rev. Lett.* **92** (2004), 198305.
- 21) Y. De Decker and A. S. Mikhailov, *J. Phys. Chem. B* **108** (2004), 14759.
- 22) M. Kiskinova “Poisoning and promotion in catalysis based on surface science concepts”, in *Studies in Surface Science and Catalysis*, vol. **70**, ser. ed. B. Delmon and J. T. Yates (Elsevier, 1992).
- 23) H. Marbach, S. Günther, B. Luersen, L. Gregoratti, M. Kiskinova and R. Imbihl, *Catal. Lett.* **83** (2002), 161.
- 24) H. Marbach, S. Günther, L. Gregoratti, M. Kiskinova and R. Imbihl, *Chem. Phys. Lett.* **364** (2002), 207.
- 25) H. Marbach, G. Lilienkamp, H. Wei, S. Günther, Y. Suchorski and R. Imbihl, *PCCP* **5** (2003), 2730.
- 26) G. W. Gardiner, *Handbook of Stochastic Methods* (Springer, Berlin, 1985).
- 27) D. G. Vlachos and M. A. Katsoulakis, *Phys. Rev. Lett.* **85** (2000), 3898.
- 28) M. A. Katsoulakis and D. G. Vlachos, *J. Chem. Phys.* **119** (2003), 9412.
- 29) J. J. Mortensen, B. Hammer and J. K. Nørskov, *Surf. Sci.* **414** (1998), 315.
- 30) A. Locatelli, A. Barinov, L. Gregoratti, L. Aballe, S. Heun and M. Kiskinova, to be published.